Astronomy & Astrophysics

The tiny globulettes in the Carina nebula★,★★

T. Grenman[1] and G. F. Gahm[2]

[1] Applied Physics, Department of Engineering Sciences & Mathematics, Luleå University of Technology, 971 87 Luleå, Sweden
  e-mail: tiia.grenman@gmail.com
[2] Stockholm Observatory, AlbaNova University Centre, Stockholm University, 106 91 Stockholm, Sweden

ABSTRACT

Context. Small molecular cloudlets are abundant in many H II regions surrounding newborn stellar clusters. In optical images these so-called globulettes appear as dark silhouettes against the bright nebular background.
Aims. We aim to make an inventory of the population of globulettes in the Carina nebula complex, and to derive sizes and masses for comparisons with similar objects found in other H II regions.
Methods. The globulettes were identified from Hα images collected at the *Hubble* Space Telescope.
Results. We have located close to 300 globulettes in the Carina complex, more than in any other region surveyed so far. The objects appear as well-confined dense clumps and, as a rule, lack thinner envelopes and tails. Objects with bright rims are in the minority, but more abundant than in other regions surveyed. Some globulettes are slightly elongated with their major axes oriented in the direction of young clusters in the complex. Many objects are quite isolated and reside at projected distances >1.5 pc from other molecular structures in the neighbourhood. No globulette coincides in position with recognized pre-main-sequence objects in the area. The objects are systematically much smaller, less massive, and much denser than those surveyed in other H II regions. Practically all globulettes are of planetary mass, and most have masses less than one Jupiter mass. The average number densities exceed 10^5 cm^{-3} in several objects. We have found a statistical relation between density and radius (mass) in the sense that the smallest objects are also the densest.
Conclusions. The population of small globulettes in Carina appears to represent a more advanced evolutionary state than those investigated in other H II regions. The objects are subject to erosion in the intense radiation field, which would lead to a removal of any thinner envelope and an unveiling of the core, which becomes more compact with time. We discuss the possibility that the core may become gravitationally unstable, in which case free-floating planetary mass objects can form.

Key words. HII regions – dust, extinction – evolution – ISM: individual objects: Carina nebula

1. Introduction

Optical images of galactic H II regions show a mix of bright and dark nebulosity. Foreground cold dust clouds obscure the bright background of warm and ionized gas. The warm plasma in these nebulæ accelerates outwards through the interaction with radiation and winds from hot and massive stars. The molecular gas is swept up and forms expanding shells, which are sculpted into complex filamentary formations, like elephant trunks, pillars that point at O stars in the nebula. Blocks of cold gas can detach from the shells and trunks and may fragment into smaller clouds that appear as dark patches on optical images of these nebulæ as noted long ago by Bok & Reilly (1947) and Thackeray (1950). The clumps may be round or shaped like tear drops, some with bright rims facing the central cluster (Herbig 1974).

A number of such H II regions have been subject to more detailed studies, and it has been found that many regions contain distinct, but very small clumps, extending over less than one to a few arcseconds. Several studies have focused on the so-called proplyds, which are photoevaporating discs surrounding very young stars (e.g. O'Dell et al. 1993; O'Dell & Wen 1994; McCaughrean & O'Dell 1996; Bally et al. 2000; Smith et al.

2003). In these studies small cloudlets without any obvious central stellar objects were also found, as also recognized by Hester et al. (1996) and Reipurth et al. (1997, 2003) from *Hubble* Space Telescope (HST) images of nebular regions.

More systematic studies of such star-less cloudlets followed, and from the surveys of more than 20 H II regions by De Marco et al. (2006), Grenman (2006), and Gahm et al. (2007; hereafter Paper I) it can be concluded that most of the objects have radii <10 kAU with size distributions that peak at ~2.5 kAU. In Paper I masses were derived from extinction measures indicating that most objects have masses <13 M_J (Jupiter masses), which currently is taken to be the domain of planetary-mass objects. This class of tiny clouds in H II regions were called *globulettes* in Paper I to distinguish them from proplyds and the much larger globules spread throughout interstellar space. We define globulettes as cloudlets with round or slightly elongated shapes with or without bright rims and/or tails.

Some globulettes are connected by thin filaments to larger molecular blocks and it is then natural to assume that isolated globulettes once detached from shells and trunks. They may also survive in this harsh environment for long times, as concluded in Paper I. Follow-up 3D numerical simulations in Kuutmann (2007) predict lifetimes of ~10^4 years, increasing with mass. Owing to the outer pressure exerted on the globulettes from surrounding warm gas, and the penetrating shock generated by photoionization, it was found that many globulettes may even

---

collapse to form brown dwarfs or planetary-mass objects before evaporation has proceeded very far. The objects are protected against rapid photoevaporation by a screen of expanding ionized gas (e.g. Dyson 1968; Kahn 1969; Tenorio-Tagle 1977). Consequently, the objects are expected to develop bright rims on the side facing the cluster because of the interaction with stellar light. In addition, the models predict that dusty tails emerge from the cloud cores. It is therefore puzzling that most globulettes lack any trace of bright rims in Hα, and that most are round, or only slightly elongated, without any trace of tails.

In a recent study by Gahm et al. (2013; hereafter Paper II), based on near-infrared imaging and radio molecular line observations of globulettes in the Rosette nebula, it was found that the objects contain dense cores, which strengthens the suggestion that many objects might collapse to form planetary-mass objects or brown dwarfs that are accelerated outwards from the nebular complex. The whole system of globulettes and trunks expands outwards from the central cluster with velocities of about 22 km s^{-1}. In the case where more compact objects are formed inside some globulettes, they will escape and become free-floating objects in the galaxy. In both the optical and radio/near-infrared surveys (Papers I and II) it was concluded that the density is relatively high even close to the surface layers, which could explain why the objects lack extensive bright rims in Hα. Some of the optically completely dark objects were discovered to have thin rims manifested in Pβ and H$_2$ emission. In a follow-up study of the near-infrared images, Mäkelä et al. (2014) found that some smaller globulettes are also crowned by thin bright rims that are not seen in Hα.

The present study is an inventory of globulettes in the Carina nebula (NGC 3372) based on images taken from the HST through a narrow-band Hα filter. Basic parameters, like size and mass, are derived and we compare the results to surveys of similar objects in other nebulae.

The Carina complex, with its extended network of bright and dark nebulosity, spans over several degrees in the sky and is one of the most prominent sites of star formation in the galaxy. More than 60 O-type stars and several young clusters (Tr 14, 15, and 16; Collinder 228 and 232; and Bochum 10 and 11) are located in the region, and more than a thousand pre-main sequence stars have been identified from optical, infrared, and X-ray surveys (e.g. Tapia et al. 2003; Ascenso et al. 2007; Sanchawala et al. 2007a,b; Smith et al. 2010a,b; Povich et al. 2011; Gaczkowski et al. 2013). The global properties of the nebular material was discussed in Smith et al. (2000), Smith & Brooks (2007), and references to studies based on observations of selected areas can be found in the comprehensive review by Smith (2008). Additional surveys from the submm range (Preibisch et al. 2011; Pekruhl et al. 2013) and the far-infrared (Preibisch et al. 2012; Roccatagliata et al. 2013) have been made more recently. The Carina nebula, in all its glory, is presented in multicolour mosaics found at the *Hubble* Space Heritage webpage.

A number of small obscuring structures in the Carina nebula were noted by Smith et al. (2003) from HST images, and were regarded as possible proplyds. However, the objects studied were found to be larger than the standard cases in the Orion nebula (Bally et al. 2000). More objects of this nature were recognized by Smith et al. (2004) who stated that their nature remains ambiguous: "analogues of Orion's proplyds, starless cometary clouds, or something in-between?" Ascenso et al. (2007), however, concluded from near-infrared imaging that these candidates do not harbour any stars. Most of these objects are globulettes by our definition and are thereby included in our list of nearly

300 globulettes. Thus the Carina complex is the richest known with regard to total number of globulettes. A number of Herbig-Haro jets emanating from embedded young stars in the region were found by Smith et al. (2010a). Most of these are related to trunks or larger fragments. However, HH 1006 is related to an isolated cloud with an embedded jet-driving source (Sahai et al. 2012; Reiter & Smith 2013). Tentative jet-signatures were also found for a few much smaller isolated clouds like HH 1011 and HHc-1.

The distance to the Carina complex has been estimated in several investigations with rather different results. A distance of 2.3 kpc has been adopted as a kind of standard (Smith 2008). Recently, Hur et al. (2012) concluded that the main stellar clusters Tr 14 and 16 are located at a distance of 2.9 kpc. We have adopted this value in the present investigation, but will discuss the implications if the complex is closer.

The paper is organized as follows. We present the fields we have searched, the objects identified, and their measured properties in Sect. 2. The results are analysed in Sect. 3 and discussed further in Sect. 4. We end with a summary in Sect. 5.

2. Objects and measurements

2.1. HST fields

The optical images of the Carina complex were downloaded from the HST archive, cycle 13 and 14 programs GO-10241 and 10475 (principal investigator N. Smith) based on observations with the ACS/WFI camera, which contains two CCDs of 2048 × 4096 pixels glued together with a small gap in between. The pixel size corresponds to ≈0.05 arcsec pixel^{-1}, and the field of view is 202 × 202 arcsec. All images selected were exposed for 1000 s through the narrow-band filter F658N, covering the nebular emission lines of Hα and [N II].

Most of the HST fields contains globulettes, and only these are listed in Table 1 with a running field number and references to target and image designations according to the HST archive. Figure 1 shows how the areas covered by HST are distributed over the region (see also Smith et al. 2010a). Two regions on opposite sides of a large V-shaped dark cloud are rather well covered by HST. The total area covered is ∼700 arcmin^2, which is larger than covered by all HST-based surveys of H II regions together, but much smaller than the area covered of the Rosette nebula in Paper I. This ground-based survey was limited to objects with radii ≥0.8 arcsec, however.

The globulettes are easily recognized as dark patches against the bright background. Most are roundish without any bright rims or halos, similar to previous surveys. A number of the elongated objects with tear-drop forms are crowned with bright rims. The Carina complex is also rich in dark irregular blocks and fragments of all sizes, some of which are very elongated and shaped like worms or long, narrow cylinders, and some show very irregular shapes. These objects, which as a rule are much larger than typical globulettes, were not included in our list of globulettes, but in Sect. 3.3 we highlight some smaller cloudlets with peculiar shapes.

The Carina nebula contains a large number of very small globulettes, down to the limit of resolution of HST, but we do not consider objects with dimensions ≤3 pixels across. Some regions contain quite isolated globulettes, while in others there are clusters of globulettes. Examples of different types of globulettes are shown in Fig. 2, where the first four rows show round and dark globulettes, which are most abundant. Round objects with bright halos are found in the fifth row followed by objects that
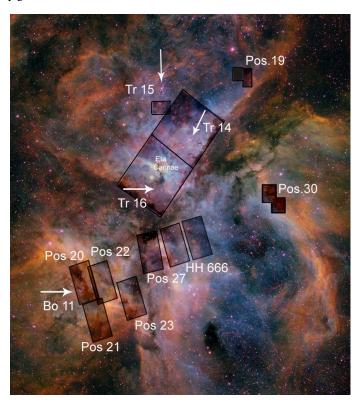
Table 1. HST archive data used.

Field/Target	RA (J2000.0)	Dec (J2000.0)	Images
1/Pos 30	10:41:27	−59:47:42	J9dk09010
2/Pos 30	10:41:38	−59:46:17	J9dk09020
3/Pos 30	10:41:40	−59:44:41	J9dka9010
4/Pos 19	10:42:23	−59:20:59	J9dk12010
5/Pos 19	10:42:48	−59:19:44	J9dk32010
6/Tr 14	10:43:07	−59:29:34	J900c1010
7/Tr 14	10:43:23	−59:32:06	J900b1010
8/Tr 14	10:43:24	−59:27:55	J900c2010
9/Tr 14	10:43:39	−59:34:37	J900a1010
10/Tr14	10:43:41	−59:30:17	J900b2010
11/Tr 14	10:43:47	−59:35:53	J90001020
12/Tr 14	10:43:55	−59:37:09	J90001010
13/HH 666	10:43:58	−59:54:39	J900a9010
14/Tr 14	10:43:59	−59:32:38	J900a2010
15/Tr 14	10:44:00	−59:28:05	J900b3010
16/HH 666	10:44:01	−59:58:42	J900b9010
17/Tr 16	10:44:05	−59:40:16	J900c5010
18/Tr 14	10:44:07	−59:33:53	J90002020
19/Tr 14	10:44:15	−59:35:09	J90002010
20/Tr 14	10:44:17	−59:30:27	J900a3010
21/Tr 14	10:44:19	−59:25:54	J900b4010
22/Tr 16	10:44:20	−59:42:48	J900b5010
23/Tr 16	10:44:22	−59:38:34	J900c6010
24/Tr 14	10:44:35	−59:33:09	J90003010
25/Tr 16	10:44:36	−59:45:19	J900a5010
26/Pos 27	10:44:40	−59:59:46	J9dk07010
27/Pos 27	10:44:43	−59:56:34	J9dk27010
28/Tr 16	10:44:44	−59:46:35	J90005020
29/Tr 16	10:44:49	−59:37:35	J900b7020
30/Tr 16	10:44:52	−59:47:51	J90005010
31/Tr 14	10:44:54	−59:31:08	J90004010
32/Tr 15	10:44:58	−59:26:50	J9dka0010
33/Tr 16	10:44:58	−59:38:47	J900b7010
34/Tr 16	10:45:12	−59:45:51	J90006010
35/Tr 16	10:45:17	−59:36:38	J900b8010
36/Tr 15	10:45:23	−59:26:59	J9dk10010
37/Tr 16	10:45:44	−59:40:34	J90008020
38/Pos 23	10:45:53	−60:08:16	j90010010
39/Pos 23	10:45:56	−60:06:42	J90010020
40/Pos 22	10:46:32	−60:05:14	J9dk23010
41/Pos 21	10:46:47	−60:09:29	J9dk22010
42/Pos 20	10:46:58	−60:06:26	J9dk01010
43/Pos 20	10:47:01	−60:03:14	J9dk21010

Fig. 1. Image of the central region of the Carina nebula, where the HST fields containing globulettes are marked. The locations of the star η Carinæ and four stellar clusters are marked. North is up and east to the left. The image spans $1.°3 \times 1.°5$ (credit: Nathan Smith, Univ. of Minnesota, NOAO, AURA, NSF).

Fig. 2. Examples of globulettes found in the Carina nebula numbered according to Table A.1. The most typical cases are the dark globulettes shown in the upper four rows followed by objects with bright halos. The last two rows show examples of elongated objects with tails, some with bright rims. We note the scales are different from panel to panel (the dimensions in arcsec are given for each object in the tables).
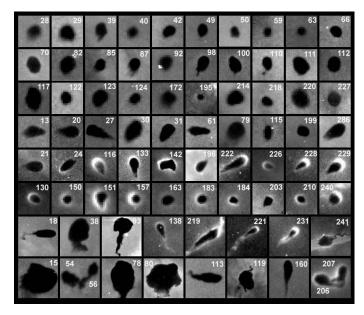
are more elongated or have developed pronounced tails, with or without bright rims.

2.2. Measurements

Central positions were measured in terms of x and y coordinates and RA and Dec according to available HST readouts. The globulettes, designated CN (as Carina nebula plus number), are listed in order of increasing RA in Table 2 showing only the first entries. The complete table is found in Table A.1. Finding charts for all fields containing globulettes are found in Fig. B.1. In these charts we have also marked some objects that we do not consider to be regular globulettes, like some clumps with peculiar shapes (see Sect. 3.3). Some larger fragments are marked as *Frag* and these features will be commented on in Sect. 4. Most globulettes have circular or slightly elliptic shapes. The semi-major and semi-minor axes are given in arcseconds in Cols. 7 and 8. These quantites are defined from an outer contour where

the intensity level has dropped to 95% of the interpolated background nebular intensity. Outside this contour, the level of noise starts to affect the definition of the boundary, but as a rule very little matter resides in the outskirts. Column 9 gives the position

Table 2. List of globulettes.

CN	Field	x	y	RA (J2000.0)	Dec (J2000.0)	α (arcsec)	β (arcsec)	PA (deg)	$\bar{r}$ (kAU)	Mass (M_J)	Remarks
1	F1	360	4020	10:41:13.3	−59:49:00	0.46	0.50		1.39	2.4	
2	F1	660	1084	10:41:18.9	−59:46:38	0.30	0.36		0.96	1.1	
3	F1	1792	3251	10:41:23.6	−59:48:35	0.38	0.40		1.13	1.3	
4	F1	1654	378	10:41:26.2	−59:46:13	0.18	0.19		0.54	0.4	
5	F1	1819	395	10:41:27.2	−59:46:15	0.19	0.27		0.67	0.6	
6	F1	2029	221	10:41:28.8	−59:46:09	0.26	0.33	23	0.86	1.2	T
7	F2	670	1907	10:41:28.9	−59:45:53	0.23	0.25	−43	0.69	*0.6*	BR, T
8	F1	2391	1935	10:41:29.1	−59:47:36	0.20	0.22		0.61	0.5	
9	F1	2156	597	10:41:29.2	−59:46:29	0.29	0.33		0.90	1.0	
10	F1	2752	1904	10:41:31.5	−59:47:38	0.54	1.46	8	2.90	*8.8*	BR, EL, T
11	F1	2604	373	10:41:32.4	−59:46:22	0.31	0.51	−38	1.19	2.0	EL
continued in Appendix A											

Notes. The symbols are defined in Sect. 2.2. The complete list of the 288 globulettes measured is presented in Appendix A.

angle of elongated objects, for which the ratio of semi-major and semi-minor axes is >1.5.

We derive the physical dimensions of the objects assuming a distance of 2.9 kpc (see Sect. 1) and define a characteristic radius, $\bar{r}$, as the mean of the semi-major and semi-minor axes expressed in kAU (Col. 10). For the determination of mass we strictly follow the procedure as described in detail in Paper I and Grenman (2006). In short, we measure the residual intensity for each pixel within a globulette relative to the interpolated bright background. This value relates to extinction due to dust at λ 6563 Å (A_α). Two extreme cases are considered: there is no foreground emission at all, or practically all the residual intensity in the darkest areas of each object is caused by foreground emission. We assume a standard interstellar reddening law (Savage & Mathis 1979) to compute the visual extinction, $A_V = 1.20\,A_\alpha$, and the column densities of molecular hydrogen, $N(H_2) = 9.4 \times 10^{20}\,A_V$, according to the relations in Bohlin et al. (1978) for each pixel assuming a standard mass ratio of gas to dust of 100, and that all hydrogen is in molecular form. The total column density is derived assuming a cosmic chemical composition. Finally, we sum over all pixels inside the contour defined above to obtain the total mass, and we select the mean of the two extreme cases defined above as a measure of the mass of each object. Column 11 gives the so derived mean mass of each globulette. The maximum and minimum masses rarely differ from the mean by more than a factor of two.

In the last column remarks about individual objects are found. Elongated globulettes are marked as EL. Some objects have developed tails or tear-drop forms and are marked T. Objects with pronounced bright rims are marked BR, and those with bright halos as BH. The derived masses for the BR and BH objects are lower limits, and their masses are set in italics in Col. 11. Symbol C indicates that the object is connected by a dark, thin filament to a larger structure, like a nearby trunk, or to another globulette (with number marked). Objects noted in Smith et al. (2003) are marked S in Col. 12 followed by the symbol they used, and two HH candidates recognized in Smith et al. (2010a) are also noted.

The derived masses are subject to other uncertainties as well. For instance, uniform density has been assumed, which is consistent (to a first approximation) with column densities derived as a function of radial position (see Paper I). However, the objects may have developed dense cores that escape detection. Another concern is the use of a normal extinction law since

larger-than-normal ratios of R have been found in certain areas (e.g. Thé et al. 1980; Smith 2002; Tapia et al. 2003; Hur et al. 2012). Since the globulettes may condense from larger clouds, they may contain larger dust grains than assumed for a normal extinction law. Finally, nebular Hα photons entering a globulette may scatter into the line of sight to the observer (e.g. Mattila et al. 2007). This effect would lead to an underestimation of mass. The effect is expected to be small, but cannot be evaluated further until more precise information exists on locations within the nebula and local radiation fields.

3. Results

We have found a total of 288 globulettes in the HST-images of the Carina complex. Most of the objects are dark without any bright rims or halos, just like those found in surveys of other H II regions. The globulettes are spread over the entire region, but are more abundant along the western part of the V-shaped dark cloud and in areas surrounding Tr 14 and 16. Examples of quite isolated globulettes can be found in Fields 10 and 25 in Fig. B.1. Clusters of globulettes are found in, for example, Fields 12 and 41 in Fig. B.1. The total number of globulettes found exceeds the number found in any other H II region. This large complex is comparatively well covered by HST observations and the number per unit area is comparable to the areas studied by De Marco et al. (2006).

3.1. Distributions of radii and masses

The left panel in Fig. 3 shows the distribution of average radii of the Carina globulettes expressed in arcsec, and in kAU in the middle panel. The bulk of the Carina globulettes have radii <1000 AU, and the distribution increases steeply towards the detection limit. Hence, the Carina globulettes are, on the whole, significantly smaller than the accumulated distribution for the seven H II regions investigated by De Marco et al. (2006), which peaks at 2.5 kAU, and with detection limits similar to ours. We note that if we instead assume a distance of 2.3 kpc to the Carina complex, as advocated by Smith (2008), then the Carina globulettes would be even smaller by ~20%.

The masses derived for the tiny globulettes in the Carina complex are consequently also, on the whole, considerably smaller than for other regions. Most of the globulettes have masses well within the domain of planetary masses. The right
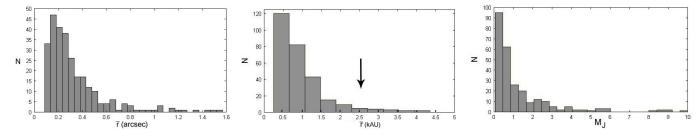
Fig. 3. *Left*: distribution of average radii as measured for all globulettes found in the Carina nebula expressed in arcsec. *Middle*: the corresponding distribution of average radii expressed in kAU and adopting a distance to the complex of 2.9 kpc. The vertical arrow marks the peak in the corresponding accumulated size distribution for objects in seven H II regions (De Marco et al. 2006). *Right*: distribution of masses for Carina globulettes less massive than 10 M_J, expressed in Jupiter masses.
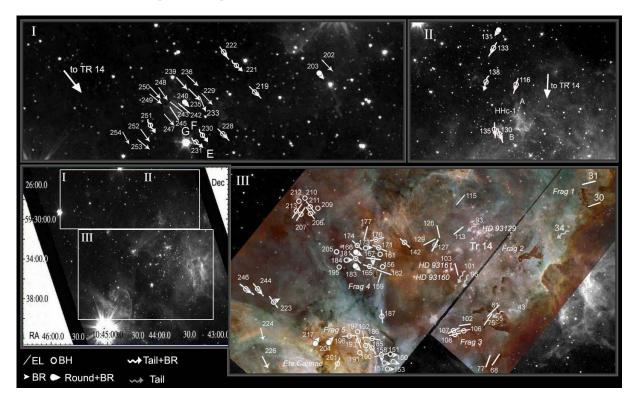

Fig. 4. In these charts the directions of the major axes of elongated objects are depicted in three areas, labelled I to III. In addition, the directions of objects with tails or bright rims present in round or elongated objects are indicated. The locations of these areas are shown in the *lower-left panel* on a map composed from Spitzer observations at 4.5 μm, This background is used in all areas, and in area III (*lower-right*) the optical image is superimposed as well. The symbols used are explained in the bottom-left corner. North is up and east to the left in these images, and CN numbers are marked according to Table A.1.

panel in Fig. 3 shows that the number of such objects increases rapidly below 3 M_J towards the detection limit. Only 4% of the Carina globulettes are more massive than 10 M_J, the most massive being CN 78 and 80 with ~130 M_J. This is in sharp contrast to the corresponding distribution in the Rosette nebula that hosts a large number of more massive clumps, some with masses of several hundred M_J (Paper I). However, even though this complex is at half the distance to the Carina complex, tiny objects with masses <2 M_J escape detection in this ground-based survey. The largest objects with masses >20 M_J are located close to and along the V-shaped dust feature (Fields 9, 11, and 12) and to the south in Field 3, Position 30 (see Fig. 1). They may represent relatively recent detachments from the nearby shell structures.

The Carina globulettes not only differ in size from those in other regions, but also in density. Their average density amounts to $\rho = 2.8 \times 10^{-19}$ g cm^{-3} compared to $\rho = 6.2 \times 10^{-20}$ g cm^{-3} for those in the Rosette nebula. In terms of number densities

of molecular hydrogen they exceed 10^5 cm^{-3} in several Carina globulettes.

3.2. Orientations

Elongated globulettes, with or without tails, line up in the same direction in certain areas, but are more randomly oriented in others. The lower left panel in Fig. 4 shows the location of three selected areas, I to III, projected on a strip composed from images obtained from Spitzer/IRAC 4.5 μm images (key No. 23695360). The two upper panels show areas I and II on the 4.5 μm background, while for area III (bottom-right panel) the optical and Spitzer images are superimposed to better illustrate the locations of stars and bright and dark nebulosity. Included are also objects with pronounced bright rims and tails and a few round objects surrounded by bright halos that are distinctly brighter at one side. Obviously, some objects classified as round may in fact

be elongated if they are oriented closer to the line of sight, and objects surrounded by bright halos flag the presence of bright rims on the remote side.

All of the objects depicted in areas I and II are oriented in about the same direction and point at the cluster Tr 14, located in area III, and it is clear that the objects have been sculpted by the interaction with photons coming from the bright stars in this cluster. It should be noted that there are also a large number of round, dark objects in these areas. In area III, elongated objects are more randomly oriented, particularly in the central part of the image. An example is CN 93 with 60 M_J in Field 18, an isolated globulette seen in projection against the cluster Tr 14. However, both the direction of the tail and the bright rim indicates that the globulette is influenced by some object east of the cluster core. Globulettes just above and along the western extension of the V-shaped dust lane (in the right part of this panel), as well as a group to the left in the panel point in the general direction of the bright nebulosity surrounding η Carina and Tr 16. Several O stars are spread over this nebulosity, and it is likely that their combined radiation caused the shaping and orientation of these elongated globulettes. In addition, we found the same predominant direction of objects in regions south of area III (not shown here).
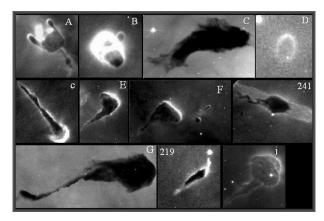
3.3. Peculiar objects

The Carina nebula hosts a large number of clouds of very irregular shape like dark worm-like filaments and larger fragments, such as the "Defiant Fingers" described by Smith et al. (2004). Some of these fragments are accompanied by smaller cloudlets with irregular shapes that most likely have eroded from the larger ones. We did not include these objects in the list of globulettes. In Fig. B.1 we have marked some larger fragments, since they might be important birth-places of globulettes (see Sect. 4).
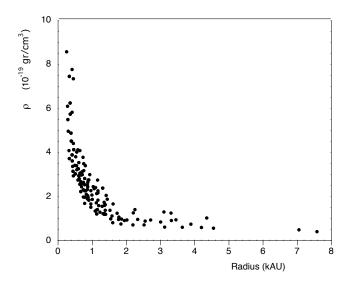
The border-line between what we define as a globulette or not is a bit arbitrary, but this is less important in our statistical analysis. Figure 5 shows some examples of cloudlets with peculiar shapes, and their locations can be found in Fig. B.1, except for j which is in an HST field void of globulettes. This object, like object c, was noted and labelled in Smith et al. (2003). Objects B and D could be similar to standard globulettes, but since B appears to be surrounded by strong Hα emission, and D is in the background behind strong foreground emission, these objects could not be measured for extinction. The other objects have peculiar dusty tails, and object A even shows three such outgrowths. These tails can be the result of erosion of elongated objects with peculiar density structure, or they may be examples of dust-enshrouded jets from embedded sources. Objects CN 219 and 241 were recognized as HH-objetcs in Smith et al. (2003), but their nature remains unclear. The objects CN 219 has a bright rim with a detached bright spot just to the north and the thin, twisted dust-tail in CN 241 is remarkable as is the surrounding, faint, and very elongated bright halo. Some of the peculiar objects in Fig. 5 deserve a closer inspection.

4. Discussion

None of the 288 globulettes coincides in position with any of the YSO candidates listed in Povich et al. (2011) and Gaczkowski et al. (2013). There are stars seen inside the boundaries of two globulettes in optical images, namely CN 138 (Fig. 2) and the object designated j in Fig. 5 in Smith et al. (2003). These stars are likely to be foreground stars, since they show no sign of IR excess judging from the Two Micron All Sky Survey

Fig. 5. Examples of objects with peculiar shapes. The objects are marked in Fig. B.1, except for object c which falls outside areas containing globulettes. This object and j are denoted in Smith et al. (2003). The images span: A 5″ × 5″, B 4″ × 4″, C 20″ × 30″, D 3″ × 3″, c 8″ × 8″, E 7″ × 10″, F 20″ × 10″, CN241 7″ × 5″, G 35″ × 18″, CN219 7″ × 7″, j 15″ × 15″.
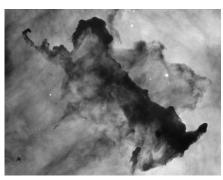
Fig. 6. Average density versus radius for all dark globulettes in the Carina complex.

(Skrutskie et al. 2006) or existing *Spitzer* images. There are no obvious proplyd candidates in our sample, except possibly for CN 219 with a jet-like extension (see Fig. 5) and listed as a Herbig-Haro object (HH 1011) in Smith et al. (2010a).

The fraction of objects with bright rims and halos is 39%, which is large compared to findings from other H II regions (De Marco et al. 2006; Paper I). In the central parts of the Carina nebula objects with bright rims even dominate over those without indicating that the interaction with the radiation field is more intense closer to the centre.

An important finding is the statistical relation between average density and radius shown in Fig. 6, where we have selected only distinctly dark objects without bright rims and halos. The smallest objects with radii <1 kAU are on average four times denser than those with radii >2 kAU. The corresponding distribution including all objects in Table A.1 shows the same general trend but with a larger scatter, and where the densities of BRs and BHs are systematically lower than the distribution in Fig. 6. This is expected since the masses for these objects are lower limits as
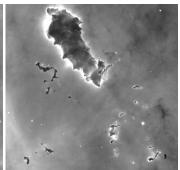
Fig. 7. Three detached fragments in the Carina nebula. *From left to right*: Fragments 1, 2, and 4 in Fields 7, 9, and 24 in Fig. B.1. These larger blocks contain denser cores, some of which appear to be detaching (see Frag. 1). Fragment 4 is surrounded by smaller cloudlets of different shapes.

pointed out in Sect. 2.2. It is likely that the distribution in Fig. 6 reflects how globulettes evolve with time.

4.1. Origin and fate

Most dark formations seen in the optical images are located in front of the central regions of bright nebulosity. For the mass estimates we have considered two extreme cases: all residual emission in the darkest parts is due to foreground emission, or there is (practically) no foreground emission. The Carina region is very complex, and it is difficult to judge how deeply embedded a given globulette is in the warm nebulosity. For the same reason it is hard to determine the geometrical distance between a given globulette and other dust formations or clusters in the area. Some globulettes are quite isolated with projected distances to the closest dust complexes of more than 1.5 pc, for example the group of globulettes in Field 14 containing Tr 14. A possible scenario is that this group is the remnant of a larger cloud that gradually eroded in the intense radiation field from Tr 14.

It was inferred in Paper I that globulettes in the Rosette nebula originate from condensations in elephant trunks and shell features. In the Carina complex there are a number of isolated, larger fragments that must have detached from shell structures long ago. Such fragments are marked in Fields 7, 9, 12, 24, and 29. Figure 7 shows examples of such fragments and all contain condensations with masses similar to those found in globulettes. Fragment 4 is surrounded by a cluster of smaller irregular fragments that appear to be leftovers from a presumably larger block that once eroded. We note that Fragment 2, which hosts several condensations, looks like a detached elephant trunk composed by a network of thin twisted filaments similar to the threaded elephant trunks discussed in Carlqvist et al. (2003).

As discussed in Paper II, the lack of distinct bright rims in Hα may be traced to a combination of several circumstances. One is that the density distributions are rather flat and that the density is high even close to the surface where the gas is in molecular form as flagged by fluorescent H_2 emission. In addition, thin Pβ emitting rims were discovered to be present in several objects, rims that in some cases appear to extend over the remote side of the objects. Such thin bright rims, not detected in Hα, were also found in several much smaller globulettes in the Rosette nebula (Mäkelä et al. 2014). Moreover, the Carina objects could be located at considerable distances from the bright UV-radiating stars, in which case the flux of exciting Lyman continuum photons is moderate producing only weak photodissociation in the outer layer at the dense surface.

The large number of quite isolated globulettes indicates that the objects have survived for a long time in the nebula. Most of these objects are tiny and dense, and unlike the larger objects they lack thin envelopes. It appears that the population of tiny globulettes in the Carina complex are in a more evolved state than those encountered in other H II regions, either because they have eroded faster in the intense radiation field, or because they are, on the whole, older. A likely scenario is that globulettes detach from larger molecular blocks, like shell structures, pillars, and fragments. Thin envelopes would gradually be lost with time, and the remnant cores may become denser with time. This scenario is further supported by the findings presented in Fig. 6 showing that the average density is inversely proportional to radius.

In Paper I we applied simple virial arguments to conclude that most globulettes in the Rosette nebula could be gravitationally unstable, especially after considering the influence of an outer pressure from the surrounding warm plasma. When applying the same analysis to the Carina globulettes we found that the globulettes are close to virial equilibrium but none is bound, even when assuming an outer pressure (thermal plus turbulence) of the same magnitude as in the Rosette complex. On the other hand, the radiation pressure exerted by light from the numerous O stars in Carina should be much higher. This pressure acts on one side of the globulettes. The derived masses are subject to uncertainties (see Sect. 2), and we note that very little extra mass is needed to confine the objects, as would be the case if they contain denser yet unresolved cores, or more speculatively, even Jupiter-sized planets. This would clarify why the globulettes appear to have survived for such a long time, as can be seen by their distribution over the nebula, where many objects are quite isolated and reside far away from larger molecular structures.

The total number of unbound planets in the Milky Way could amount to several hundred billion (Sumi et al. 2011). Globulettes in H II regions may be an additional source of such free-floating planetary-mass objects besides an origin in circumstellar protoplanetary disks from where they are ejected (e.g. Veras et al. 2009).

5. Conclusions

We have made an inventory of globulettes in the Carina nebula complex based on existing HST narrow-band Hα images. A total of 288 globulettes were listed and measured for size, mass, and density. Most objects are either round or slightly elongated, and many of the latter are oriented in the direction of massive young clusters in the area. We discuss why only a minority have developed bright Hα emitting rims and/or tails, and we note that there is no evidence so far of any embedded young stars.

The Carina globulettes are, on the whole, much smaller and less massive than those recognized from HST surveys of a number of other H II regions. Practically all are of planetary mass, and most have masses less than one Jupiter mass. The corresponding mean densities are much higher than in other regions, exceeding number densities of 10^5 cm^{-3} in several objects. We found a statistical relation between average density and size in the sense that the smallest globulettes are also the densest. Globulettes may detach from larger blocks of molecular gas, like isolated fragments, elephant trunks, and shell structures, after which their thinner envelopes evaporate and leave denser cores, which may become even more compressed with time.

From virial arguments we conclude that the objects are not bound unless they contain a bit more mass than inferred from the derived mean mass. Most of the tiny objects are quite isolated and located at projected distances of >1.5 pc from the closest larger molecular structures, which indicates that the objects can survive for long times in the nebula. We speculate that the objects might contain denser cores or even planetary-mass objects that already have formed in their interior.

We suggest that the Carina globulettes are a more evolved state than the larger and less dense objects that are abundant in other H II regions. Globulettes in H II regions may be one source of the large number of free-floating planetary-mass objects that has been estimated to exist in the Galaxy.

References

Ascenso, J., Alves, J., Vicente, S., & Lago, M. T. V. T. 2007, A&A, 476, 199
Bally, J., O'Dell, C. R., & McCaughrean, M. J. 2000, AJ, 119, 2919
Bok, B. J., & Reilly, E. J. 1947, ApJ, 105, 255
Bohlin, R. C., Savage, B. D., & Drake, J. F. 1978, ApJ, 224, 132
Carlqvist, P., Gahm, G. F., & Kristen, H. 2003, A&A, 403, 399
De Marco, O., O'Dell, C. R., Gelfond, P., Rubin, R. H., & Glover, S. C. O. 2006, AJ, 131, 2580
Dyson, J. E. 1968, A&AS, 1, 388
Gaczkowski, B., Preibisch, T., Ratzka, T., et al. 2013, A&A, 549, A67
Gahm, G. F., Grenman, T., Fredriksson, S., & Kristen, H. 2007, AJ, 133, 1795 (Paper I)
Gahm, G. F., Persson, C. M., Mäkelä , M. M., & Haikala, L. K. 2013, A&A, 555, A57 (Paper II)
Grenman, T. 2006, Licentiate thesis, Luleå University of Technology, Sweden (ISSN 1402-1757)
Herbig, G. 1974, PASP, 86, 604
Hester. J. J., Scowen, P.A., Sankrit, R., et al. 1996, AJ, 111, 2349
Hur, H., Sung, H., & Bessell, M.S. 2012, AJ, 143, 41
Kahn, F. D. 1969, Physica, 41, 172
Kuutmann, A. 2007, Master's Thesis, Dep. of Astronomy, Stockholm University, Sweden
Mäkelä, M. M., Haikala, L. K., & Gahm, G. F. 2014, A&A, submitted
Mattila, K., Juvela, M., & Lehtinen, K. 2007, A&A, 654, L131
McCaughrean, M. J., & O'Dell, C. R. 1996, AJ, 111, 1977
O'Dell, C. R., & Wen, Z. 1994, ApJ, 436, 194
O'Dell, C. R., Wen, Z., & Hu, X. 1993, ApJ, 410, 696
Pekruhl, S., Preibisch, T., Schuller, F., & Menten, K. 2013, A&A, 550, A29
Povich, M. S., Smith, N., Majewski, S. R., et al. 2011, ApJS, 194, 14
Preibisch, T., Schuller, F., Ohlendorf, H., et al. 2011, A&A, 525, A92
Preibisch, T., Roccatagliata, V., Gaczkowski, B., & Ratzka, T. 2012, A&A, 531, A132
Reipurth, B., Corporon, P., Olberg, M., & Tenorio-Tagle, G. 1997, A&A, 327, 1185
Reipurth, B., Raga, A., & Heathcote, S. 2003, AJ, 126, 1925
Reiter, M., & Smith, N. 2013, MNRAS, 433. 2226
Roccatagliata, V., Preibisch, T., Ratzka, T., & Gaczkowski, B. 2013, A&A, 554, A6
Sahai, R., Güsten, R., & Morris, M. R., 2012, ApJ, 761, L21
Sanchawala, K., Chen, W.-P., Ojha, D., et al. 2007a, ApJ, 667, 963
Sanchawala, K., Chen, W.-P., Lee H.-T., et al. 2007b, ApJ, 656, 462
Savage, B. D., & Mathis, J. S. 1979, ARA&A, 17, 73
Skrutskie, M. F., Cutri, R. M., Stiening., R., et al. 2006, AJ, 131, 1163
Smith, N. 2002, MNRAS, 331, 7
Smith, N. 2008, Handbook of Star Forming Regions, Vol. II: The Southern Sky, ASP Monograph Publ., ed. Bo Reipurth, 5, 138
Smith, N., & Brooks, K. J. 2007, MNRAS, 379, 1279
Smith, N., Egan M. P., Carey, S., et al. 2000, ApJ, 532, L145
Smith, N., Bally, J., & Morse, J. A. 2003, ApJ, 587, L105
Smith, N., Barbá, R. H., & Walborn, N. R. 2004, MNRAS, 351, 1457
Smith, N., Bally, J., & Walborn, N. R. 2010a, MNRAS, 405, 1153
Smith, N., Povich, N. S., Whitney, B. A., et al. 2010b, MNRAS, 406, 952
Sumi, T., Kamiya, K., Bennett, D. P., et al. 2011, Nature, 473, 349
Tapia, M., Roth, M., Vázquez, R. A., & Feinstein, A. 2003, MNRAS, 339, 44
Tenorio-Tagle, G. 1977, A&A, 54, 517
Thackeray, A. D. 1950, MNRAS, 110, 524
Thé, A. D., Bakker, R., & Tjin A Djie, H. R. E. 1980, A&A, 89, 209
Veras, D. Crepp, J. R., & Ford, E. B. 1998, A&A, 332, L5

Appendix A: Properties of the globulettes in the Carina complex

Table A.1. List of globulettes in the Carina nebula complex.

CN	Field	x	y	RA (J2000.0)	Dec (J2000.0)	α (arcsec)	β (arcsec)	PA (degr.)	$\bar{r}$ (kAU)	Mass (M_J)	Remarks
1	F1	360	4020	10:41:13.3	−59:49:00	0.46	0.50		1.39	2.4	
2	F1	660	1084	10:41:18.9	−59:46:38	0.30	0.36		0.96	1.1	
3	F1	1792	3251	10:41:23.6	−59:48:35	0.38	0.40		1.13	1.3	
4	F1	1654	378	10:41:26.2	−59:46:13	0.18	0.19		0.54	0.4	
5	F1	1819	395	10:41:27.2	−59:46:15	0.19	0.27		0.67	0.6	
6	F1	2029	221	10:41:28.8	−59:46:09	0.26	0.33	23	0.86	1.2	T
7	F2	670	1907	10:41:28.9	−59:45:53	0.23	0.25	−43	0.69	*0.6*	BR, T
8	F1	2391	1935	10:41:29.1	−59:47:36	0.20	0.22		0.61	0.5	
9	F1	2156	597	10:41:29.2	−59:46:29	0.29	0.33		0.90	1.0	
10	F1	2752	1904	10:41:31.5	−59:47:38	0.54	1.46	8	2.90	*8.8*	BR, EL, T
11	F1	2604	373	10:41:32.4	−59:46:22	0.31	0.51	−38	1.19	2.0	EL
12	F2	1207	1745	10:41:32.6	−59:45:50	0.31	0.35	−15	0.96	1.5	T
13	F1	2808	667	10:41:33.4	−59:46:38	0.36	0.70	13	1.54	2.7	EL
14	F2	1694	1606	10:41:35.9	−59:45:48	0.39	0.46		1.23	1.8	
15	F3	2659	851	10:41:44.9	−59:43:44	1.47	1.67		4.55	40	
16	F3	2806	1494	10:41:45.2	−59:44:17	0.52	0.71		1.78	4.5	
17	F3	2706	964	10:41:45.2	−59:43:50	0.20	0.21		0.59	0.5	
18	F3	2972	933	10:41:46.9	−59:43:51	0.69	1.82	12	3.64	22	EL, T
19	F3	3527	1546	10:41:49.8	−59:44:26	0.31	0.44		1.09	1.3	
20	F3	3656	1501	10:41:50.7	−59:44:25	0.36	0.67	6	1.49	*2.5*	BR, EL
21	F2	3781	272	10:41:51.2	−59:45:02	0.64	1.00	10	2.38	*5.6*	BR, EL
22	F4	2772	3493	10:42:20.7	−59:19:45	0.35	0.40		1.09	*1.6*	BR
23	F5	2719	1339	10:42:43.7	−59:20:16	0.18	0.20		0.55	0.4	
24	F5	1880	938	10:42:48.7	−59:20:42	0.35	0.72	−5	1.55	*2.8*	BR, EL
25	F5	1242	524	10:42:52.4	−59:21:08	0.25	0.47	−3	1.04	*1.5*	BR, EL
26	F8	1029	1467	10:43:15.9	−59:28:07	0.13	0.14		0.39	0.2	
27	F6	3938	1861	10:43:16.1	−59:28:31	0.52	1.22	33	2.52	8.5	EL, T, C
28	F8	973	1754	10:43:16.8	−59:28:19	0.21	0.27		0.70	0.8	
29	F6	2697	3970	10:43:17.6	−59:30:33	0.26	0.28		0.78	0.9	
30	F7	1960	1480	10:43:19.9	−59:31:45	0.24	0.38	20	0.90	1.5	EL
31	F7	3105	479	10:43:22.1	−59:30:31	0.36	0.61	23	1.41	4.3	EL
32	F7	2177	3163	10:43:27.5	−59:32:47	0.35	0.41		1.10	2.4	
33	F13	3571	682	10:43:31.4	−59:55:20	0.49	0.75	−13	1.80	*4.0*	BH, EL
34	F7	2583	3776	10:43:32.0	−59:33:00	0.23	0.26	36	0.71	0.7	T
35	F7	2883	4143	10:43:35.1	−59:33:06	0.19	0.25		0.64	0.5	
36	F7	3181	3863	10:43:35.6	−59:32:46	0.23	0.24		0.68	0.7	
37	F7	3360	4002	10:43:37.1	−59:32:46	0.11	0.13		0.35	0.2	
38	F9	3329	499	10:43:39.1	−59:32:57	0.95	1.33		3.31	34	S*e*
39	F9	3552	393	10:43:39.8	−59:32:46	0.39	0.51		1.31	4.0	S*e*
40	F10	1537	3364	10:43:43.8	−59:31:24	0.19	0.21		0.58	0.6	
41	F11	1933	2248	10:43:46.4	−59:36:05	0.18	0.25		0.62	0.5	
42	F11	1935	2353	10:43:46.8	−59:36:09	0.35	0.46		1.17	2.6	
43	F11	2066	2364	10:43:47.6	−59:36:06	0.26	0.34	−10	0.87	1.3	T
44	F9	2972	3165	10:43:47.6	−59:34:56	0.33	0.40		1.06	2.1	
45	F9	3255	2797	10:43:47.7	−59:34:33	0.13	0.13		0.38	0.2	
46	F9	3325	2858	10:43:48.3	−59:34:33	0.11	0.13		0.35	0.2	
47	F9	2914	3633	10:43:49.1	−59:35:16	0.13	0.14		0.39	0.2	
48	F9	2893	3668	10:43:49.1	−59:35:18	0.11	0.12		0.33	0.1	
49	F10	2378	3919	10:43:50.4	−59:31:18	0.36	0.44		1.16	3.2	
50	F9	3229	3794	10:43:51.4	−59:35:14	0.30	0.41		1.03	2.0	
51	F12	506	3746	10:43:52.5	−59:39:03	0.56	0.78		1.94	5.0	
52	F16	3116	1570	10:43:52.9	−59:58:49	0.27	0.34		0.88	1.0	
53	F11	2489	3191	10:43:53.0	−59:36:27	0.21	0.30		0.74	0.8	
54	F11	2530	3187	10:43:53.2	−59:36:25	0.33	0.48		1.17	2.7	C to 56
55	F11	2573	3152	10:43:53.3	−59:36:23	0.12	0.16	39	0.41	0.3	T
56	F11	2554	3196	10:43:53.3	−59:36:25	0.26	0.35		0.88	1.4	C to 54
57	F11	2589	3155	10:43:53.4	−59:36:22	0.12	0.13		0.36	0.2	
58	F11	2873	2777	10:43:53.5	−59:35:59	0.25	0.29		0.78	1.0	
59	F11	2611	3162	10:43:53.6	−59:36:22	0.13	0.15		0.41	0.2	

Notes. The symbols are described in Sect. 2.2.

Table A.1. continued.

CN	Field	x	y	RA (J2000.0)	Dec (J2000.0)	α (arcsec)	β (arcsec)	PA (degr.)	$\bar{r}$ (kAU)	Mass (M_J)	Remarks
60	F11	2952	2770	10:43:53.9	−59:35:56	0.15	0.17		0.46	0.3	
61	F11	2569	3315	10:43:53.9	−59:36:29	0.27	0.70	−6	1.38	2.7	EL
62	F11	2874	2959	10:43:54.2	−59:36:06	0.16	0.24		0.58	0.4	
63	F11	2722	3170	10:43:54.2	−59:36:19	0.13	0.14		0.39	0.2	
64	F12	830	3731	10:43:54.2	−59:38:53	0.44	0.47		1.32	2.1	
65	F11	2595	3360	10:43:54.2	−59:36:31	0.15	0.16		0.45	0.2	
66	F16	2341	102	10:43:54.5	−60:00:11	0.33	0.41		1.07	2.2	
67	F12	891	3782	10:43:54.7	−59:38:54	0.17	0.18		0.51	0.3	
68	F12	827	3883	10:43:54.8	−59:38:59	0.75	1.12	−10	2.71	14	EL
69	F12	1124	3501	10:43:54.9	−59:38:35	0.36	0.42		1.13	1.5	
70	F16	2304	190	10:43:54.9	−60:00:08	0.42	0.57		1.44	4.2	
71	F11	2766	3381	10:43:55.2	−59:36:26	0.13	0.16		0.42	0.2	
72	F12	1251	3451	10:43:55.4	−59:38:30	0.39	0.50		1.29	2.5	
73	F11	2833	3366	10:43:55.5	−59:36:24	0.12	0.16		0.41	0.2	
74	F11	2790	3454	10:43:55.6	−59:36:29	0.20	0.23		0.62	0.5	
75	F11	2796	3536	10:43:55.9	−59:36:32	0.18	0.33	−9	0.74	0.7	EL
76	F11	2805	3527	10:43:56.0	−59:36:31	0.18	0.26		0.64	0.5	
77	F12	1049	3910	10:43:56.1	−59:38:54	0.73	1.34	−16	3.00	17	EL
78	F11	2606	3914	10:43:56.4	−59:36:53	2.06	2.80		7.05	128	C
79	F17	1970	196	10:43:56.4	−59:39:03	1.16	1.22		3.45	29	
80	F11	2844	3613	10:43:56.6	−59:36:33	2.30	2.93		7.58	132	
81	F17	2057	149	10:43:56.7	−59:38:58	0.63	0.65		1.86	4.7	
82	F14	2761	894	10:43:56.7	−59:31:32	0.22	0.28		0.73	1.1	
83	F12	1222	3852	10:43:56.8	−59:38:47	0.34	0.44		1.13	1.3	
84	F14	2839	813	10:43:56.8	−59:31:26	0.13	0.15		0.41	0.2	
85	F12	1406	3654	10:43:56.9	−59:38:33	0.70	0.82		2.20	10	
86	F17	2182	172	10:43:57.5	−59:38:56	0.44	0.50		1.36	3.0	
87	F12	1314	3927	10:43:57.5	−59:38:47	0.71	0.84		2.25	12	
88	F14	3211	691	10:43:58.1	−59:31:10	0.13	0.21		0.49	0.3	
89	F11	3786	2786	10:43:58.4	−59:35:32	0.13	0.15		0.41	0.2	
90	F17	2303	274	10:43:58.5	−59:38:56	0.58	0.81		2.02	5.8	
91	F14	3214	863	10:43:58.9	−59:31:16	0.12	0.12		0.35	0.2	
92	F14	2726	1454	10:43:58.9	−59:31:54	0.22	0.27		0.71	0.8	
93	F18	2146	258	10:43:59.6	−59:32:38	1.31	1.69	5	4.35	63	T, Si
94	F18	384	3025	10:44:01.1	−59:35:22	0.14	0.16		0.44	0.2	
95	F14	2903	1866	10:44:01.6	−59:32:04	0.09	0.11		0.29	0.1	
96	F18	575	2990	10:44:01.9	−59:35:15	0.18	0.26	−40	0.64	0.8	T
97	F14	2890	2055	10:44:02.4	−59:32:12	0.12	0.13		0.36	0.2	
98	F14	2865	2085	10:44:02.4	−59:32:14	0.37	0.46		1.20	*3.2*	BR, Sf
99	F18	559	3151	10:44:02.5	−59:35:22	0.20	0.22		0.61	0.5	
100	F14	2994	2059	10:44:02.8	−59:32:08	0.36	0.54		1.31	*4.0*	Sf
101	F18	660	3153	10:44:03.0	−59:35:19	0.17	0.30	−13	0.68	0.6	EL, T
102	F12	3489	2374	10:44:03.1	−59:36:40	0.12	0.23	3	0.51	0.3	EL
103	F18	722	3146	10:44:03.3	−59:35:17	0.15	0.23	11	0.55	0.5	EL, T
104	F18	708	3183	10:44:03.4	−59:35:19	0.17	0.21		0.55	0.5	
105	F12	3420	2634	10:44:03.8	−59:36:53	0.10	0.10		0.29	0.1	
106	F12	3392	2729	10:44:03.9	−59:36:57	0.10	0.23	27	0.48	*0.2*	BH, EL
107	F12	3409	2742	10:44:04.1	−59:36:57	0.10	0.16	7	0.38	*0.2*	BH, EL
108	F12	3447	2703	10:44:04.2	−59:36:55	0.10	0.17	21	0.38	*0.2*	BH, EL
109	F12	3450	2789	10:44:04.5	−59:36:58	0.12	0.19	22	0.45	*0.2*	BH, EL
110	F17	2657	1400	10:44:04.7	−59:39:32	0.33	0.45		1.13	2.3	
111	F17	2603	1490	10:44:04.8	−59:39:37	0.49	0.62		1.61	5.2	
112	F17	2587	1545	10:44:04.9	−59:39:40	0.43	0.50		1.35	3.2	
113	F14	2686	2944	10:44:05.2	−59:32:52	0.26	0.69	43	1.38	3.2	EL
114	F17	2737	1427	10:44:05.3	−59:39:30	0.11	0.10		0.30	0.1	
115	F14	3623	2009	10:44:05.8	−59:31:46	0.14	0.24	44	0.55	0.5	EL
116	F15	2760	2864	10:44:06.4	−59:28:13	0.17	0.35	−31	0.75	*0.8*	BH, EL
117	F14	2847	3192	10:44:07.0	−59:32:56	0.26	0.38		0.93	1.8	
118	F14	3190	2832	10:44:07.2	−59:32:31	0.08	0.09		0.25	0.1	
119	F17	2961	1710	10:44:07.6	−59:39:35	1.22	1.68		4.20	33	

Table A.1. continued.

CN	Field	x	y	RA (J2000.0)	Dec (J2000.0)	α (arcsec)	β (arcsec)	PA (degr.)	$\bar{r}$ (kAU)	Mass (M_J)	Remarks
120	F14	3189	2936	10:44:07.6	−59:32:35	0.11	0.12		0.33	0.2	
121	F14	3203	3000	10:44:07.9	−59:32:37	0.13	0.14		0.39	0.2	
122	F14	2861	3513	10:44:08.5	−59:33:08	0.19	0.23		0.61	0.6	
123	F14	3194	3190	10:44:08.7	−59:32:45	0.23	0.29		0.75	1.1	
124	F14	3272	3217	10:44:09.3	−59:32:43	0.18	0.23		0.59	0.5	
125	F14	2906	3805	10:44:09.9	−59:33:17	0.12	0.14		0.38	0.2	
126	F14	3011	3781	10:44:10.4	−59:33:13	0.20	0.39	16	0.86	0.9	EL
127	F14	2991	3827	10:44:10.5	−59:33:16	0.28	0.49	−5	1.12	*2.3*	BH, EL
128	F14	2909	3956	10:44:10.6	−59:33:23	0.11	0.12		0.33	0.2	
129	F14	2977	3907	10:44:10.7	−59:33:19	0.15	0.39	43	0.78	0.8	EL
130	F20	1107	2190	10:44:12.6	−59:31:03	0.19	0.29	20	0.70	*0.7*	BH, EL
131	F21	1458	1517	10:44:12.8	−59:25:53	0.17	0.21		0.55	*0.4*	BR
132	F21	1441	1599	10:44:13.0	−59:25:57	0.16	0.20		0.52	*0.4*	
133	F21	1347	1758	10:44:13.2	−59:26:06	0.38	0.89	−11	1.84	*3.8*	BH, EL
134	F19	1781	2650	10:44:15.0	−59:35:41	0.21	0.23		0.64	0.6	
135	F20	1747	2070	10:44:15.3	−59:30:38	0.13	0.23	3	0.52	*0.3*	BH, EL
136	F22	1814	1588	10:44:16.8	−59:42:36	0.10	0.14		0.35	*0.2*	BH
137	F22	2295	1451	10:44:18.8	−59:42:16	0.41	0.52	−26	1.35	*2.5*	BH, T
138	F20	3991	352	10:44:19.1	−59:28:20	0.32	0.67	−24	1.44	*2.7*	BH, EL, T
139	F22	2338	1531	10:44:19.4	−59:42:18	0.11	0.15		0.38	*0.2*	BH
140	F28	287	834	10:44:19.9	−59:33:12	0.09	0.10		0.28	0.1	
141	F28	245	1067	10:44:20.6	−59:33:23	0.13	0.16		0.42	0.2	
142	F28	439	1398	10:44:22.9	−59:33:30	0.41	0.90	−17	1.90	*10*	BH, EL
143	F26	3864	1397	10:44:28.1	−60:00:08	0.18	0.26		0.64	0.5	
144	F26	3874	1486	10:44:28.1	−60:00:03	0.26	0.34		0.87	1.2	
145	F26	3875	1543	10:44:28.2	−60:00:00	0.51	0.71		1.77	4.0	
146	F26	3811	1412	10:44:28.5	−60:00:07	0.27	0.32		0.86	1.1	
147	F26	3810	1434	10:44:28.5	−60:00:06	0.24	0.27		0.74	0.8	
148	F26	3759	1382	10:44:28.8	−60:00:09	0.23	0.28		0.74	0.8	
149	F26	3623	506	10:44:28.9	−60:00:53	0.25	0.32		0.83	0.9	
150	F23	2896	2906	10:44:29.1	−59:38:40	0.11	0.12		0.33	*0.2*	BH
151	F23	3070	2960	10:44:30.2	−59:38:37	0.13	0.16		0.42	*0.3*	BH
152	F28	552	3222	10:44:30.6	−59:34:41	0.17	0.25		0.61	0.5	
153	F23	2756	3560	10:44:31.1	−59:39:10	0.18	0.33		0.74	*0.6*	BH
154	F28	503	3487	10:44:31.3	−59:34:53	0.12	0.13		0.36	0.2	
155	F26	3610	3069	10:44:31.4	−59:58:47	0.23	0.23		0.67	0.5	C
156	F28	657	3347	10:44:31.6	−59:34:43	0.12	0.16		0.41	*0.2*	BH
157	F23	2990	3452	10:44:31.9	−59:39:01	0.11	0.11		0.32	*0.1*	BH
158	F23	3159	3340	10:44:32.2	−59:38:49	0.12	0.22	24	0.49	*0.3*	BH, EL
159	F28	650	3554	10:44:32.4	−59:34:51	0.18	0.30	−11	0.69	0.6	EL
160	F27	3512	750	10:44:32.5	−59:57:30	0.42	1.19	6	2.33	9.1	EL, T
161	F28	1561	2363	10:44:32.6	−59:33:36	0.10	0.12		0.32	*0.1*	BH
162	F28	671	3584	10:44:32.6	−59:34:52	0.11	0.21	44	0.46	0.3	EL
163	F29	156	490	10:44:32.6	−59:37:36	0.15	0.20		0.51	*0.5*	BH
164	F26	3436	3148	10:44:32.6	−59:58:44	0.24	0.23		0.68	0.7	C
165	F28	731	3521	10:44:32.7	−59:34:47	0.25	0.50	−5	1.09	*1.6*	BH, EL
166	F28	1180	2970	10:44:32.9	−59:34:12	0.11	0.15		0.38	*0.2*	BR
167	F28	960	3282	10:44:32.9	−59:34:31	0.26	0.47	−37	1.06	*1.3*	BH, EL
168	F27	3434	856	10:44:33.1	−59:57:25	0.14	0.16		0.44	0.2	
169	F26	2931	196	10:44:33.1	−60:01:14	0.34	0.43		1.12	1.8	
170	F26	3400	863	10:44:33.3	−59:57:25	0.11	0.12		0.33	0.1	
171	F27	989	3389	10:44:33.5	−59:34:34	0.11	0.22	−13	0.48	*0.2*	BH, EL
172	F26	2859	463	10:44:33.9	−60:01:01	0.50	0.55		1.52	3.6	
173	F28	1165	3251	10:44:33.9	−59:34:24	0.18	0.27		0.65	*0.6*	BH
174	F28	1147	3298	10:44:34.0	−59:34:26	0.14	0.32	−4	0.67	*0.4*	BH, EL
175	F26	2899	971	10:44:34.1	−60:00:36	0.46	0.73	2	1.73	4.8	EL, T
176	F28	1231	3217	10:44:34.1	−59:34:20	0.12	0.24	21	0.52	*0.3*	BH, EL
177	F28	1250	3203	10:44:34.2	−59:34:19	0.31	0.78	−29	1.58	3.3	EL
178	F26	2733	168	10:44:34.4	−60:01:17	0.15	0.16		0.45	0.3	
179	F29	455	586	10:44:34.5	−59:37:30	0.13	0.15		0.41	0.4	

Table A.1. continued.

CN	Field	x	y	RA (J2000.0)	Dec (J2000.0)	α (arcsec)	β (arcsec)	PA (degr.)	$\bar{r}$ (kAU)	Mass (M_J)	Remarks
180	F28	1585	2904	10:44:34.8	−59:33:57	0.11	0.13		0.35	0.2	BH
181	F28	1330	3301	10:44:35.0	−59:34:21	0.10	0.24	−9	0.49	0.2	BH, EL
182	F26	2599	499	10:44:35.6	−60:01:01	0.18	0.19		0.54	0.4	
183	F28	1340	3499	10:44:35.8	−59:34:29	0.12	0.15		0.39	0.3	BR
184	F28	1707	3005	10:44:35.9	−59:33:58	0.19	0.26		0.65	0.6	BH
185	F29	306	1298	10:44:36.8	−59:38:03	0.15	0.34	9	0.71	0.8	BH, EL
186	F29	385	1214	10:44:36.8	−59:37:57	0.12	0.19	−42	0.45	0.3	BH, EL
187	F29	325	1329	10:44:37.0	−59:38:03	0.13	0.22	−13	0.51	0.5	BH, EL
188	F29	967	666	10:44:37.5	−59:37:17	0.10	0.12		0.32	0.1	
189	F26	2389	1025	10:44:37.5	−60:00:37	0.60	0.67		1.84	3.5	
190	F29	389	1433	10:44:37.8	−59:38:05	0.18	0.34	21	0.75	1.0	BH, EL, T
191	F29	416	1430	10:44:37.9	−59:38:04	0.09	0.10		0.28	0.1	BH
192	F29	601	1217	10:44:37.9	−59:37:50	0.13	0.17	9	0.44	0.3	BR.EL
193	F29	466	1381	10:44:37.9	−59:38:01	0.14	0.23	7	0.54	0.3	BH, EL
194	F29	1203	581	10:44:38.3	−59:37:06	0.12	0.14		0.38	0.2	
195	F28	2194	3098	10:44:38.8	−59:33:47	0.09	0.10		0.29	0.1	BH
196	F29	763	1319	10:44:39.2	−59:37:49	0.26	0.45	6	1.03	2.0	BH, EL
197	F29	877	1190	10:44:39.2	−59:37:40	0.10	0.12		0.32	0.1	BH
198	F29	1014	1365	10:44:40.6	−59:37:43	0.15	0.20		0.51	0.3	
199	F25/28	1945	3616	10:44:41.3	−59:46:26	1.22	1.46		3.89	33	
200	F25	3596	1558	10:44:42.1	−59:44:14	0.35	0.59	2	1.36	2.3	EL
201	F33	380	1177	10:44:45.2	−59:39:07	0.15	0.25	−26	0.58	0.4	BH, EL
202	F32	1780	3807	10:44:46.8	−59:26:25	0.18	0.30	−1	0.70	0.7	BR, EL
203	F32	1884	3764	10:44:47.0	−59:26:30	0.25	0.33		0.84	1.1	BR
204	F33	1657	317	10:44:48.1	−59:37:53	0.27	0.34		0.88	1.1	BR
205	F28	3952	3839	10:44:51.0	−59:33:25	0.11	0.10		0.30	0.1	BH
206	F31	1558	3034	10:44:55.0	−59:32:03	0.23	0.37	31	0.87	1.0	BH, EL, C to 207
207	F31	1578	3041	10:44:55.2	−59:32:03	0.18	0.41	−7	0.81	0.8	BH, EL, C to 206
208	F28	2749	4107	10:44:55.5	−59:47:38	0.22	0.29		0.74	0.6	
209	F31	1729	2933	10:44:55.5	−59:31:54	0.12	0.17		0.42	0.2	BH
210	F31	1744	2954	10:44:55.7	−59:31:54	0.18	0.24		0.61	0.5	BH
211	F31	1776	2936	10:44:55.8	−59:31:53	0.15	0.28	−8	0.62	0.5	BH, EL
212	F31	1822	2927	10:44:56.0	−59:31:51	0.11	0.13		0.35	0.2	BH
213	F31	1839	2938	10:44:56.1	−59:31:51	0.24	0.50	−10	1.07	1.3	BH, EL
214	F33	2034	1833	10:44:56.4	−59:38:40	0.23	0.29		0.75	1.0	
215	F30	2894	2278	10:44:57.1	−59:47:36	0.37	0.42		1.15	1.6	
216	F34	634	493	10:44:58.1	−59:45:30	0.24	0.31		0.80	0.8	BH
217	F33	2984	1488	10:44:59.7	−59:37:56	0.21	0.26		0.68	0.6	BR
218	F33	3039	2209	10:45:03.0	−59:38:22	0.17	0.20		0.54	0.4	
219	F32	2175	991	10:45:05.0	−59:26:57	0.34	1.23	44	2.28	4.0	BH, EL, HH 1011
220	F34	1926	694	10:45:05.8	−59:45:00	0.27	0.33		0.87	1.0	
221	F32	1901	849	10:45:06.0	−59:26:44	0.17	0.39	36	0.81	0.6	BH, EL, T
222	F32	1800	790	10:45:06.5	−59:26:39	0.22	0.63	35	1.22	1.4	BH, EL
223	F35	1157	892	10:45:07.0	−59:36:22	0.19	0.32	−4	0.74	0.8	BH, EL
224	F33	3463	2708	10:45:07.3	−59:38:28	0.09	0.12	9	0.30	0.1	BR, EL
225	F33	3876	2237	10:45:07.4	−59:37:56	0.13	0.17		0.43	0.2	
226	F33	2807	3660	10:45:08.0	−59:39:25	0.11	0.21	23	0.46	0.2	BR, EL
227	F34	1339	2233	10:45:08.7	−59:46:19	0.83	0.93		2.55	11	
228	F36	3883	3930	10:45:10.2	−59:28:18	0.12	0.31	41	0.62	0.4	BH, EL
229	F36	2492	3336	10:45:14.8	−59:27:11	0.26	0.45	41	1.03	1.5	BR, EL
230	F36	3665	3179	10:45:15.2	−59:28:10	0.23	0.94	31	1.70	1.0	BH, EL, T
231	F36	3991	3108	10:45:15.5	−59:28:26	0.17	0.30	−8	0.68	0.4	BH, EL, T
232	F34	2953	1788	10:45:15.5	−59:45:14	0.45	0.65		1.60	2.5	
233	F36	3003	3106	10:45:16.0	−59:27:37	0.10	0.19	35	0.42	0.2	BR, EL
234	F34	3018	1878	10:45:16.2	−59:45:15	0.53	0.98	−14	2.19	5.6	EL
235	F36	2999	3076	10:45:16.2	−59:27:37	0.11	0.23	35	0.49	0.3	BR, EL
236	F36	2080	3045	10:45:16.9	−59:26:52	0.12	0.21	−4	0.49	0.3	BR, EL
237	F36	2850	2967	10:45:17.0	−59:27:03	0.09	0.18	36	0.39	0.2	BR, EL
238	F36	2053	2993	10:45:17.3	−59:26:50	0.11	0.18	37	0.42	0.2	BR, EL
239	F36	2086	2949	10:45:17.6	−59:26:52	0.19	0.34	38	0.77	1.0	BR, EL

Table A.1. continued.

CN	Field	x	y	RA (J2000.0)	Dec. (J2000.0)	α (arcsec)	β (arcsec)	PA (degr.)	$\bar{r}$ (kAU)	Mass (M_J)	Remarks
240	F36	3557	2638	10:45:18.8	−59:28:07	0.43	0.49		1.33	2.3	BR
241	F34	4031	1315	10:45:19.4	−59:44:23	0.86	1.29	−15	3.12	14	EL, T, HH 900
242	F36	3013	2526	10:45:19.8	−59:27:40	0.11	0.20	−5	0.45	0.5	EL
243	F36	2815	2471	10:45:20.3	−59:27:31	0.22	0.33	−8	0.80	1.3	EL
244	F35	3833	803	10:45:20.3	−59:34:54	0.19	0.56	−6	1.09	1.9	BH, EL
245	F36	2956	2448	10:45:20.4	−59:27:38	0.12	0.20	−4	0.46	0.3	EL
246	F35	3925	862	10:45:21.0	−59:34:53	0.11	0.22	−21	0.48	0.4	BH, EL
247	F36	2947	2037	10:45:23.1	−59:27:39	0.17	0.35	41	0.75	0.5	BR, EL
248	F36	2438	2035	10:45:23.4	−59:27:14	0.15	0.26	34	0.59	0.5	BR, EL
249	F36	2642	2011	10:45:23.4	−59:27:24	0.14	0.25	−6	0.56	0.4	BR, EL
250	F36	2426	1969	10:45:23.8	−59:27:13	0.10	0.20	41	0.44	0.2	BR, EL,
251	F36	3344	1606	10:45:25.7	−59:28:01	0.11	0.19	44	0.43	0.2	BH, EL, T
252	F36	3446	1332	10:45:27.4	−59:28:07	0.12	0.41	36	0.77	0.4	BR, EL
253	F36	3855	1259	10:45:27.6	−59:28:28	0.20	0.57	−7	1.12	0.9	BR, EL
254	F36	3465	722	10:45:31.4	−59:28:10	0.10	0.25	28	0.51	0.2	BR, EL
255	F37	1063	1293	10:45:43.3	−59:41:48	0.17	0.32	−8	0.71	0.5	BH, EL
256	F37	1218	1373	10:45:49.3	−59:41:20	0.19	0.22		0.59	0.5	
257	F37	2123	1452	10:45:49.6	−59:41:23	0.24	0.32		0.81	0.9	T
258	F38	1950	772	10:45:52.4	−60:09:22	0.94	1.20		3.10	29	
259	F39	2083	1920	10:45:56.4	−60:06:50	0.25	0.37		0.90	1.0	
260	F39	1727	1822	10:45:58.5	−60:07:00	0.39	0.54		1.35	2.2	C
261	F40	3160	2494	10:46:25.4	−60:04:46	0.23	0.34	24	0.83	0.8	BH, T
262	F40	1860	859	10:46:32.5	−60:06:16	0.17	0.52	11	1.00	0.8	BH, EL
263	F40	1829	2265	10:46:34.0	−60:05:07	0.22	0.74	13	1.39	1.4	BH, EL
264	F40	1684	2025	10:46:34.8	−60:05:20	0.18	0.39	13	0.83	0.9	BH, EL
265	F40	1595	3374	10:46:36.6	−60:04:13	0.29	0.35		0.93	0.9	BH, C
266	F40	1099	2480	10:46:39.1	−60:05:01	0.18	0.36	6	0.78	0.6	BH, EL
267	F40	1183	3446	10:46:39.4	−60:04:13	0.18	0.28		0.67	0.4	BH
268	F40	548	2567	10:46:42.8	−60:05:01	0.12	0.21	10	0.48	0.3	BH, EL
269	F40	572	3295	10:46:43.3	−60:04:24	0.22	0.35	27	0.83	0.7	BH, EL
270	F40	536	3228	10:46:43.5	−60:04:28	0.15	0.31	24	0.67	0.5	BH, EL
271	F41	2754	3454	10:46:44.0	−60:08:16	0.35	0.64	−38	1.44	2.0	BH, EL
272	F42	4047	547	10:46:44.2	−60:07:29	0.23	0.41	−43	0.93	0.6	BH, EL
273	F41	2206	3203	10:46:47.4	−60:08:33	0.25	0.29		0.78	0.6	
274	F41	1750	609	10:46:48.0	−60:10:44	0.18	0.28	40	0.67	0.5	EL
275	F41	2193	3922	10:46:48.2	−60:07:57	0.40	0.68	−25	1.7	3.3	BH, EL
276	F41	2118	3648	10:46:48.4	−60:08:11	0.25	0.32		0.83	0.7	BR
277	F41	1974	3499	10:46:49.2	−60:08:20	0.32	0.34		0.96	1.0	
278	F41	1870	3499	10:46:49.9	−60:08:20	0.60	0.91	32	2.19	5.3	BH, EL
279	F41	1788	3611	10:46:50.6	−60:08:15	0.37	0.39		1.10	1.4	BH
280	F41	1664	2864	10:46:50.7	−60:08:53	0.25	0.29		0.78	0.7	
281	F43	3479	1455	10:46:51.4	−60:03:35	0.34	0.47	7	1.17	2.9	BR, EL, T
282	F41	1472	3476	10:46:52.5	−60:08:24	0.20	0.26		0.67	0.5	
283	F43	2949	1487	10:46:54.9	−60:03:37	0.31	0.50	26	1.17	2.2	EL, C to 268
284	F43	2933	1486	10:46:55.0	−60:03:38	0.26	0.42	15	0.99	1.5	EL, C to 267
285	F43	2818	1519	10:46:55.8	−60:03:37	0.13	0.14		0.39	0.2	
286	F42	2371	3032	10:46:57.7	−60:05:38	0.82	1.47	35	3.32	25	EL
287	F43	2498	3796	10:47:00.0	−60:01:46	0.25	0.45	−23	1.02	1.3	BH, EL
288	F43	2411	4092	10:47:00.9	−60:01:32	0.32	0.37		1.00	1.4	

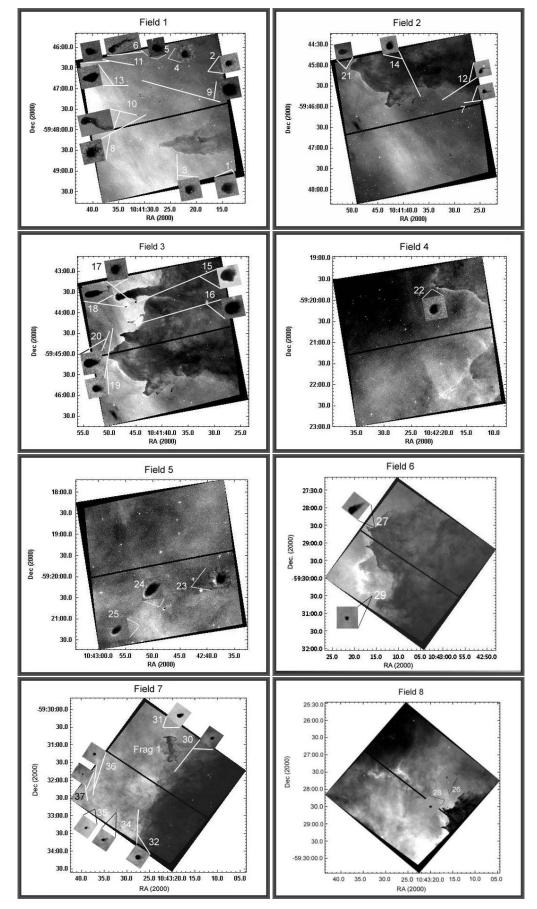# Appendix B: Atlas of fields with globulettes

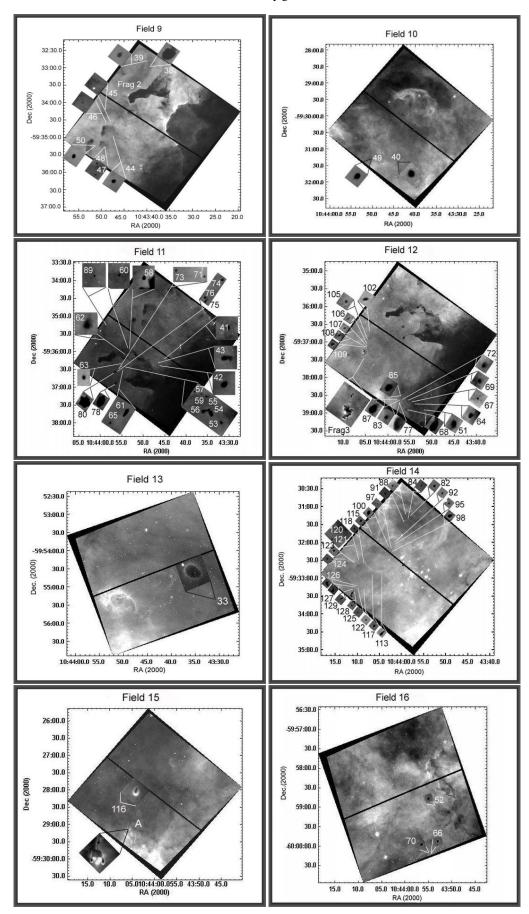**Fig. B.1.** Fields 1 to 8 with object designation and inserted enlargements of globulettes.

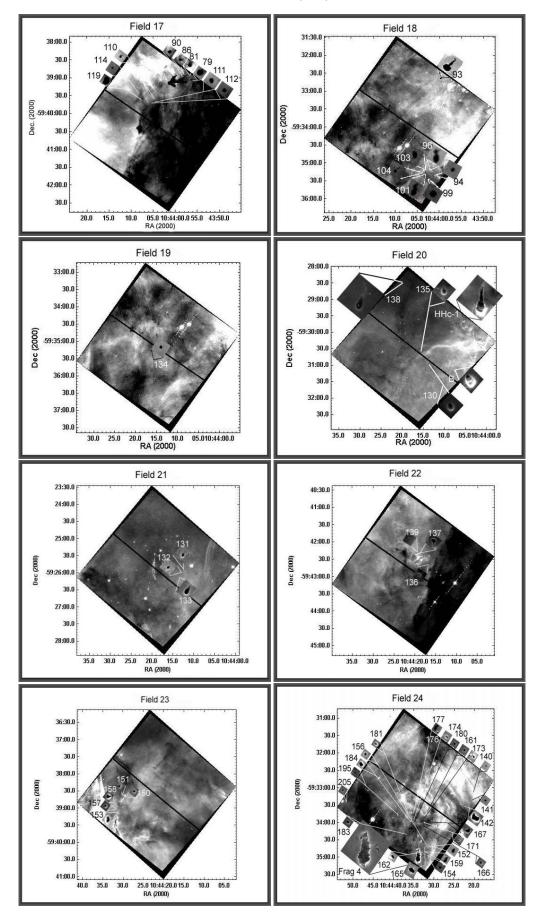**Fig. B.1.** continued. Fields 9 to 16.
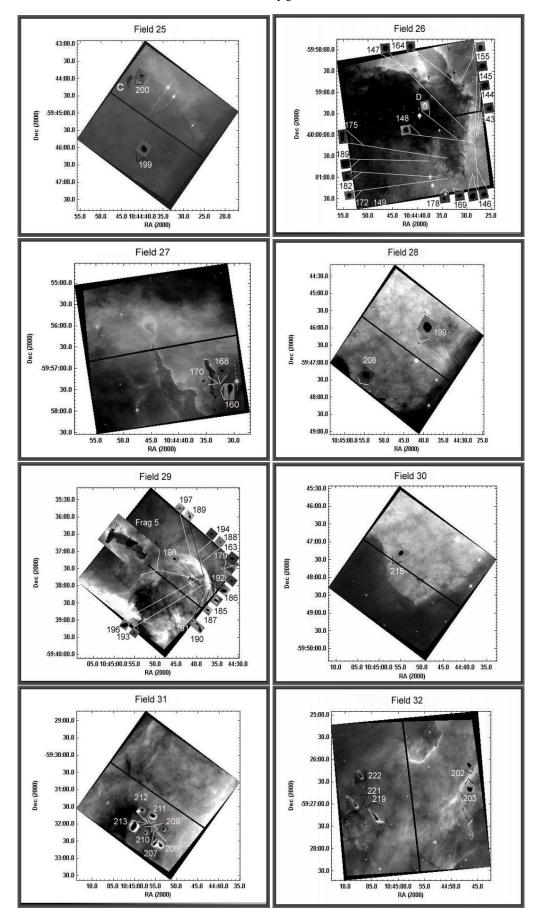
Fig. B.1. continued. Fields 17 to 24.
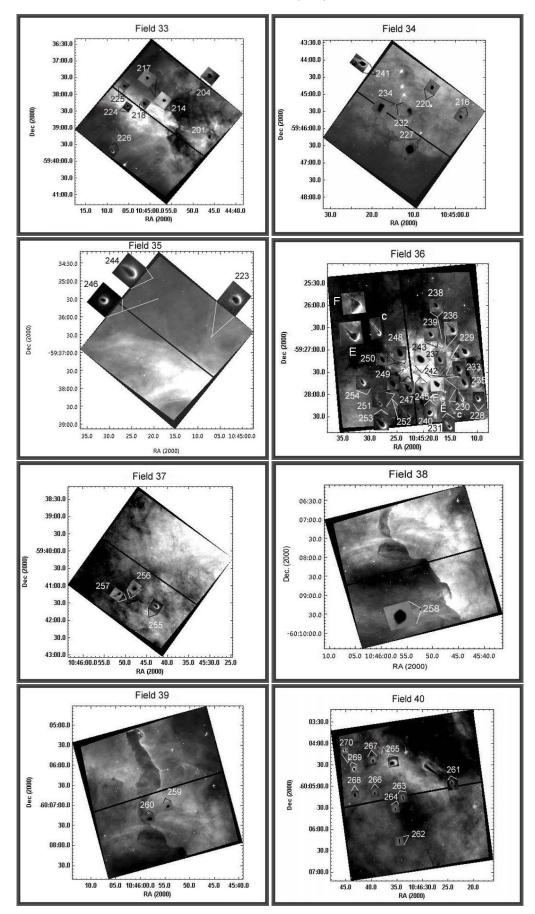
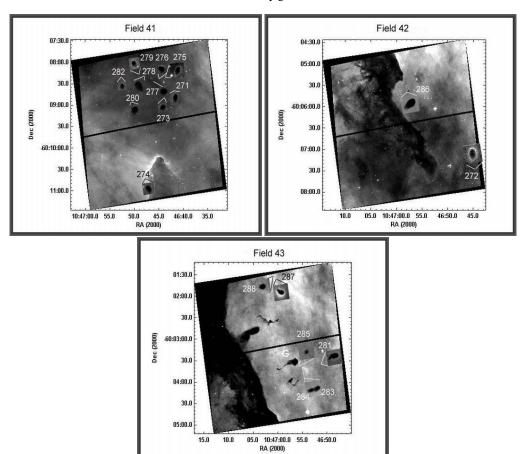**Fig. B.1.** continued. Fields 25 to 32.

Fig. B.1. continued. Fields 33 to 40.

Fig. B.1. continued. Fields 41 to 43.